

Two plaquette-singlet phases in the Shastry-Sutherland compound $\text{SrCu}_2(\text{BO}_3)_2$

Yi Cui,^{1,2} Kefan Du,¹ Zhanlong Wu,¹ Shuo Li,³ Pengtao Yang,³ Ying Chen,¹ Xiaoyu Xu,¹ Hongyu Chen,¹ Chengchen Li,¹ Juanjuan Liu,^{1,2} Bosen Wang,³ Wenshan Hong,³ Shiliang Li,^{3,4} Zhiyuan Xie,^{1,2} Jinguang Cheng,^{3,4} Rong Yu,^{1,2} and Weiqiang Yu^{1,2,*}

¹*School of Physics and Beijing Key Laboratory of Opto-electronic Functional Materials & Micro-nano Devices, Renmin University of China, Beijing, 100872, China*

²*Key Laboratory of Quantum State Construction and Manipulation (Ministry of Education), Renmin University of China, Beijing, 100872, China*

³*Beijing National Laboratory for Condensed Matter Physics and Institute of Physics, Chinese Academy of Sciences, Beijing, 100190, China*

⁴*School of Physical Sciences, University of Chinese Academy of Sciences, Beijing, 100190, China*

The nature of the high-pressure plaquette-singlet (PS) phase of $\text{SrCu}_2(\text{BO}_3)_2$ remains enigmatic. In this work, we revisit the high-pressure ^{11}B NMR study and identify two distinct coexisting gapped PS states within the NMR spectra. In addition to the previously reported full-plaquette phase, a second PS phase is discerned, characterized by a slightly lower resonance frequency and larger spin-lattice relaxation rates in its ordered phase. Notably, this second phase exhibits enhanced spin fluctuations in its precursor liquid state above the transition temperature. The volume fraction of this phase increases significantly with pressure, reaching approximately 70% at 2.65 GPa. Furthermore, at 2.4 GPa, a field-induced quantum phase transition from the PS phase to an antiferromagnetic phase is observed around 5.5 T, with a scaling behavior of $1/T_1 \sim T^{0.6}$ near the transition field. This behavior suggests a continuous or nearly continuous nature for the field-induced transition. Our findings provide experimental evidence for the long-sought empty-plaquette singlet phase in $\text{SrCu}_2(\text{BO}_3)_2$ within the framework of the Shastry-Sutherland model, thus establishing a promising platform for future studies of deconfined quantum criticality in this model system.

Introduction. Magnetic frustration induces strong quantum fluctuations and competing quantum phases, sparking significant interest in the search for emergent quantum phases and quantum phase transitions (QPTs). A notable example is the Shastry-Sutherland model (SSM) on a square lattice [1], which features competing interdimer antiferromagnetic (AFM) interactions J and intradimer AFM interactions J' between spins. As the ratio $\alpha = J/J'$ increases, numerical simulations predict a sequence of quantum phase transitions: the ground state evolves from a dimerized singlet (DS) phase to a plaquette-singlet (PS) phase- also known as the empty-plaquette (EP) phase [2, 3] and culminates in an ordered AFM phase [2, 4–8]. A key theoretical prediction in this model is the presence of a deconfined quantum critical point (DQCP) [9] at the EP- AFM phase transition, suggesting a continuous order-to-order QPT beyond the Landau paradigm [10, 11]. The realization of this lattice model in material form is of great interest, offering the possibility to experimentally test for a DQCP with enhanced symmetries and fractional excitations, such as spinons, at the critical point [9, 12–17]. Studies of deconfined quantum criticality have extended to various physical systems [18–23].

$\text{SrCu}_2(\text{BO}_3)_2$ is an antiferromagnet containing Shastry-Sutherland interactions [24, 25], where exchange interactions are $J \approx 46$ K and $J' \approx 75$ K at ambient pressure. With increasing pressure, the ratio α grows, making $\text{SrCu}_2(\text{BO}_3)_2$ an ideal candidate to explore pressure-tuned quantum phases [26]. High-pressure NMR studies have indicated a field-induced PS–AFM transition with a nearby DQCP [27], while zero-field specific heat measurements suggest a pressure-induced first-order PS –AFM tran-

sition [28]. Recent simulations of the SSM also predict a pressure-induced first-order or weakly first-order EP AFM phase transition [29, 30], challenging the proposed DQCP scenario for the SSM. Notably, inelastic neutron scattering (INS) and NMR studies on $\text{SrCu}_2(\text{BO}_3)_2$ indicate that its high-pressure PS phase adopts a full-plaquette (FP) pattern [26, 27], with half of the dimers located within four-site singlets [3, 31]. This observation contrasts with the EP phase, where the local plaquette singlet lacks the J' dimer bond, as expected in the SSM.

To further investigate the EP phase and the potential DQCP in $\text{SrCu}_2(\text{BO}_3)_2$, we revisited high-pressure ^{11}B NMR studies on this material. Through careful spectral analysis, we identified macroscopic phase coexistence, evidenced by the splitting of the NMR line into double peaks at low temperatures. The high-frequency peak corresponds to a precursor liquid phase below 3.5 K and an ordered FP phase below 1.8 K [27]. The low-frequency peak, previously unstudied, reveals enhanced spin fluctuations characteristic of a PL phase, reflected in a peaked NMR Knight shift K_n and a large spin-lattice relaxation rate $1/T_1$ before the system transitions into another PS phase at lower temperatures. The volume fraction of this second PS phase increases with pressure, from 20% at 1.85 GPa to 70% at 2.65 GPa. A field-induced PS–AFM transition is observed around 5.5 T at 2.4 GPa, with the spin-lattice relaxation rate following a scaling behavior, $1/T_1 \sim T^{0.6}$ near the transition field. Comparing our results with recent simulations of the SSM [29], we propose that this second PS phase corresponds to the EP phase. This discovery provides a valuable opportunity to investigate quantum criticality and phase transitions within the SSM by examining $\text{SrCu}_2(\text{BO}_3)_2$ under

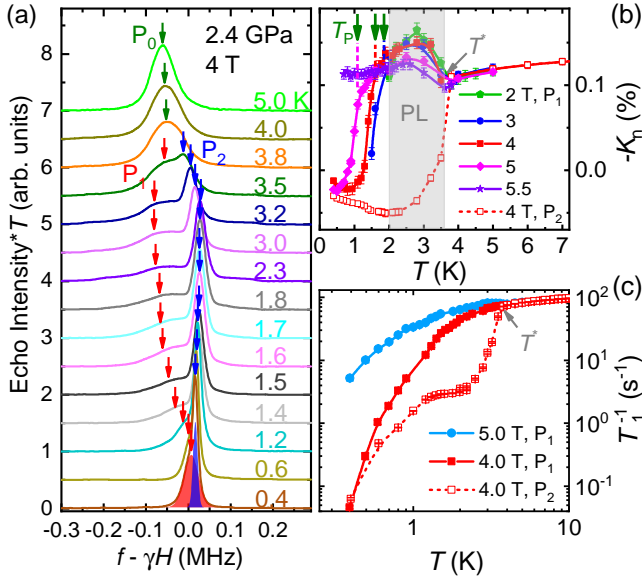


FIG. 1. ^{11}B NMR spectra at 2.4 GPa. (a) Spectra measured at 4 T with decreasing temperatures (data vertically shifted for clarity). The peaks are labeled as P_0 , P_1 , and P_2 , indicating their respective positions in the spectra. Spectrum at 0.4 K is fit to a double Gaussian function, with the resulting red and blue lineshapes shown in the figure. (b) K_n for the different peaks as functions of temperatures, measured at various magnetic fields. The PS ordering temperature T_P is identified by a sharp drop in $-K_n$ for the P_1 peak upon cooling. T^* marks the onset temperature of the PL phase (shaded area). (c) $1/T_1$ as functions of temperatures, measured at the positions of the identified peaks.

high pressure.

Phase separation and two plaquette-singlet phases. ^{11}B NMR measurements were conducted on a single crystal with the magnetic field applied along the crystalline c -axis. Pressures up to 2.4 GPa were achieved using a NiCrAl piston cell (PC), while a cubic anvil cell (CAC) was employed to reach 2.65 GPa. The ^{11}B NMR spectra, measured using the spin-echo technique (excluding satellite lines), were obtained at 2.4 GPa over a temperature range from 5 K down to 0.4 K under a constant magnetic field of 4 T, as shown in Fig. 1(a).

At temperatures of 3.8 K and above, a single resonance line, labeled P_0 , is observed. Upon cooling, the resonance splits into two distinct peaks, denoted as P_1 and P_2 : P_1 is a low-frequency, broad peak, while P_2 is a high-frequency, narrow peak. Notably, the position of P_1 initially shifts to lower frequencies, then to higher frequencies as the temperature decreases. In contrast, P_2 shows a monotonic frequency increase with decreasing temperature, the behavior of the FP phase reported in previous studies [3, 27, 31]. Knight shifts, K_n , for both P_1 and P_2 were calculated for comparison. Given the negative hyperfine coupling constant $A_{hf} \approx -0.259 \text{ T}/\mu_B$ [27, 32], values of $-K_n$ are plotted as functions of temperature at different magnetic fields, as shown in Fig. 1(b).

For P_1 at 4 T, $-K_n$ exhibits an upturn around 3.5 K, con-

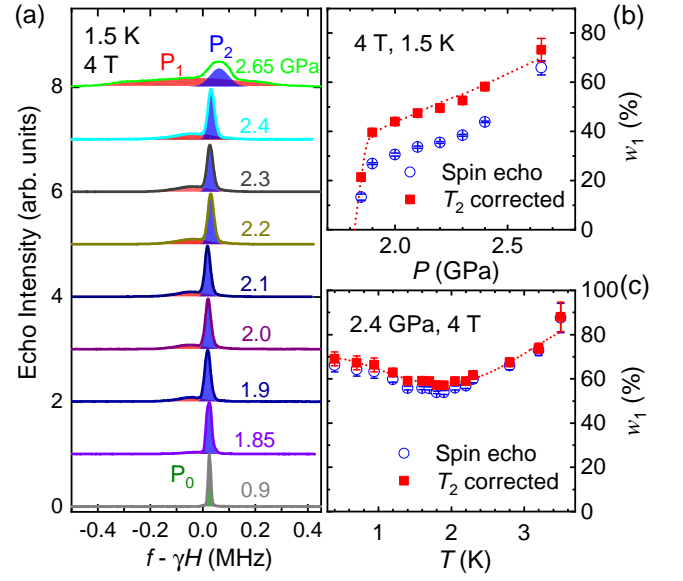


FIG. 2. **Volume fraction of different PL phases.** (a) NMR spectra measured at 1.5 K and 4 T under increasing pressure (data vertically shifted for clarity). The green, blue, and red shaded areas represent the results of single or double Gaussian fits, corresponding to the peak positions P_0 , P_1 , and P_2 , respectively. (b) w_1 (volume fraction of P_1) as a function of pressure, measured at 4 T and 1.5 K. Open circles represent raw data calculated from the spin-echo intensity with different pulse lengths, while filled squares denote data corrected for the T_2 effect (see text). (c) Temperature dependence of w_1 measured at 2.4 GPa and a fixed field of 4 T. Spin-echo data shown in (b) and (c) were collected with different pulse lengths.

trasting with a sharp downturn in P_2 at the same temperature. We define this upturn onset temperature as T^* , marking the emergence of a PL phase, where no phase transition is detected. A peak in $-K_n$ appears around 2.5 K, slightly above the transition temperature (indicated by downward arrows in Fig. 1(b)), signaling a region of enhanced magnetic fluctuations prior to entering the ordered PS phase. Below 1.65 K, $-K_n$ decreases sharply, indicating a transition to the gapped PS phase, which is characterized by a reduction in uniform magnetic susceptibility. This ordering temperature is identified as T_P . Similar trends in K_n for P_1 are observed under varying magnetic fields, with T_P decreasing as the field strength increases. Values of T_P and T^* for various fields are plotted in the phase diagram shown in Fig. 4.

The spin-lattice relaxation rates, $1/T_1$, measured at peaks P_1 and P_2 , are compared in Fig. 1(c). In the PL phase, for $T < T^*$, $1/T_1$ at P_1 shows a clear field dependence. Specifically, $1/T_1$ measured at P_1 under magnetic fields of 4 T and 5 T decreases moderately as the temperature drops from 10 K to 2 K.

In the PL phase, P_1 and P_2 are distinctly separated. For P_2 , the change in K_n indicates a pronounced reduction in magnetic susceptibility below T^* , followed by a nearly constant value below 2.5 K [27]. Similarly, the spin-lattice relaxation rate $1/T_1$ measured at P_2 shows a sharp, monotonic drop be-

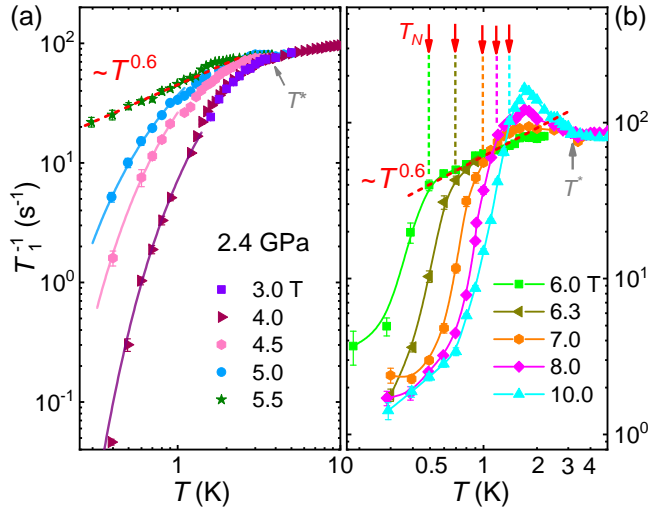


FIG. 3. **Spin-lattice relaxation rates measured on P_1 .** (a) $1/T_1$ as functions of temperatures, measured under low magnetic fields. Solid lines represent fits to the thermal activation function, given by $1/T_1 \sim T^{0.6} e^{-\Delta/T}$. (b) $1/T_1$ measured at high magnetic fields. The Néel temperature T_N is indicated by a sharp drop in $1/T_1$. Dotted lines in both (a) and (b) serve as guides, representing the scaling behavior $1/T_1 \sim T^{0.6}$ at 5.5 T and 6 T, respectively.

low T^* . Notably, the spectral separation between P_1 and P_2 becomes minimal as temperature decreases well below T_P , as the magnetic Knight shift in both phases approaches zero.

Volume fraction of coexisting phases. We further investigate the evolution of peaks P_1 and P_2 with pressure, measured at a constant field of 4 T and a fixed temperature of 1.5 K, as shown in Fig. 2(a). At 0.9 GPa, a single peak is observed. However, for pressures at and above 1.85 GPa, a double-peak structure emerges. The spectra are fitted using a double-Gaussian function, with each spectral component represented by red and blue shaded regions. From these fits, it is evident that the relative spectral weight of P_1 increases with pressure compared to that of P_2 .

Using these fits, we calculate the volume fraction of the P_1 phase as its spectral weight relative to the total spectral weight, denoted as w_1 . Correspondingly, the volume fraction of P_2 is evaluated as $w_2 = 1 - w_1$. The evolution of w_1 with pressure in the ordered phase is shown in Fig. 2(b), where it exhibits a rapid increase between 1.8 GPa and 1.9 GPa, followed by a more gradual rise with further pressure increase. To account for the influence of the spin-spin relaxation rate, $1/T_2$, on spin-echo intensity, all data are corrected for the T_2 effect and replotted in Fig. 2(b).

The value of w_1 increases monotonically with pressure, rising from approximately 20% at 1.85 GPa to 70% at 2.65 GPa, indicating that the P_1 phase is increasingly favored at higher pressures. Spectral measurements conducted at various temperatures under a fixed pressure of 2.4 GPa and a field of 4 T show a slight increase in w_1 below 1.8 K, as shown in Fig. 2(c). We also confirm that at each pressure, the variation in w_1 with magnetic field up to 6 T is negligible (data not

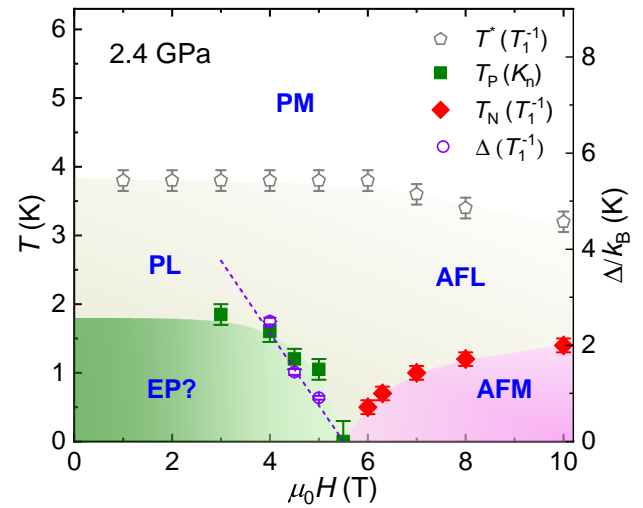


FIG. 4. **Phase diagram deduced from P_1 at 2.4 GPa.** T_N and T_P denote the transition temperatures of the ordered AFM and PS (likely the EP) phase, respectively. T^* marks the onset temperature of the PL phase at low field and the antiferromagnetic-liquid phase at high field. Δ (right axis) represents the energy gap determined within the plaquette-singlet phase. The dotted line fits to $\Delta(H) = g\mu_B(H_C - H)$.

shown).

Field-induced PS–AFM transition in P_1 . The temperature dependence of $1/T_1$ was measured under various magnetic fields at a fixed pressure of 2.4 GPa, as shown in Fig. 3(a)-(b). At low temperatures, $1/T_1$ increases with field strength from 3 T to 5.5 T but decreases from 6 T to 10 T, indicating a transition from the PS phase to the AFM phase [27].

At 5.5 T, the absence of a downturn in $1/T_1$ down to 0.3 K suggests that the PS–AFM transition field is close to this value. In the PL phase, $1/T_1$ follows a power-law dependence, $1/T_1 \sim T^{0.6}$, over the temperature range from 0.3 K to 1.5 K at 5.5 T [Fig. 3(a)] and from 0.5 K to 2 K at 6.0 T [Fig. 3(b)].

For fields below 5 T, $1/T_1$ below T_P shows thermally activated behavior, as expected for the PS phase. To account for the observed $1/T_1 \sim T^{0.6}$ at the QPT, we use the relation $1/T_1 \sim T^{0.6} e^{-\Delta/T}$, as indicated by the solid fit lines in Fig. 3(a) for fields from 4 T to 5 T. The energy gaps Δ extracted from these fits are included in the phase diagram in Fig. 4. All values of Δ fit a linear function, $\Delta = g\mu_B(H_C - H)$, with a g -factor of 2.28 [24] and a critical field parameter $H_C \approx 5.5$ T. By linear extrapolation, we obtain $\Delta \approx 8.28$ K at zero field, consistent with the 8.5 K gap reported from specific heat measurements [28].

For fields of 6 T and above, the low-temperature data follow a gapless behavior [Fig. 3(b)], indicating a gapless AFM phase induced by field-driven Bose-Einstein condensation (BEC). The Néel temperature T_N is identified by the onset of a sharp drop in $1/T_1$, marked by downward arrows in the figure. The values of T_N increase monotonically from 0.5 K at 6 T to 1.5 K at 10 T. Below T^* , a broad peak in $1/T_1$ appears around 1.7 K across all fields above 6 T, suggesting the emergence of

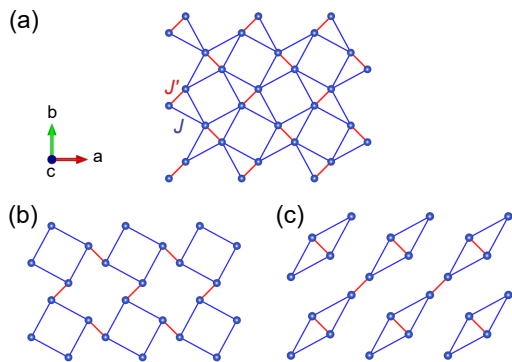


FIG. 5. **Exchange couplings and two PS phases in $\text{SrCu}_2(\text{BO}_3)_2$.** (a) Schematic drawing of major magnetic interactions J and J' among Cu^{2+} moments. (b) Illustration of an EP phase, with local singlets forming on the squares enclosed by solid lines. (c) Illustration of an FP phase, with local singlets forming on the diamonds enclosed by solid lines.

quasi-static AFM order, which we describe as an antiferromagnetic liquid (AFL).

Using the extracted values of T^* , T_P , and T_N from P_1 , we construct an (H, T) phase diagram, as shown in Fig. 4. The results reveal field suppression of the PS phase and the emergence of a field-induced AFM phase, with the PS–AFM QPT occurring near 5.5 T. Notably, the gap-closing field determined from $1/T_1$ aligns with the disappearance of T_P observed from the Knight shift K_n , as shown in Fig. 4. In comparison, the phase diagram based on P_2 [27] shows a similar critical field to that found in the present work. However, the $1/T_1$ and K_n measurements for P_1 and P_2 exhibit markedly different temperature dependencies, as illustrated in Fig. 1(b) and Fig. 1(c).

Discussions. The successful differentiation of the two phases through macroscopic coexistence in this study leverages the local probe nature of NMR. As shown in Fig. 2(b), with the volume fractions of P_1 and P_2 each exceeding 50% across the measured pressure range, both P_1 and P_2 should be regarded as distinct phases rather than contributions from domain walls of either P_1 or P_2 .

To gain further insight, we compare our results with reported tensor network calculations for the SSM, where a prominent peak in C/T at $T \approx 0.04J'$ indicates a highly fluctuating PL phase [29]. Our K_n measurements for P_1 show a peak around 2.5 K, consistent with the calculations, given $J' \approx 50$ K at the current pressure [29]. Thus, we propose that the phase associated with P_1 corresponds to the EP phase in the SSM, as indicated in the phase diagram (Fig. 4). In contrast, the monotonic decrease in $-K_n$ and $1/T_1$ below 3.5 K ($0.07J'$) for P_2 shows no sign of enhanced fluctuations, suggesting that interactions beyond the SSM may be relevant [33].

A key question is how to explain the macroscopic coexistence and evolving volume fractions of the two plaquette phases within the same compound. Figure 5 illustrates the

exchange couplings in $\text{SrCu}_2(\text{BO}_3)_2$ and the proposed EP and FP phases. The primary difference between these phases is that, in the FP phase, half amount of the dimer bonds linked by J' are enclosed within local four-site singlets (diamonds), whereas in the EP phase, none of these bonds are enclosed (squares). This contrast implies that the DS phase competes more strongly with the EP phase than with the FP phase. At pressures slightly above the first-order DS–PS phase transition point (1.8 GPa) [34], incomplete melting of dimer singlets may favor the FP phase over the EP phase. With further pressure increases, the EP phase could become favored, as required by the SSM. Additionally, higher pressures often introduce greater non-hydrostaticity, which may further destabilize interactions necessary to sustain the FP phase.

Interestingly, INS data on $\text{SrCu}_2(\text{BO}_3)_2$ supports only the FP phase, measured at a pressure just above the DS–PS boundary [26]. In contrast, C_m/T data for $\text{SrCu}_2(\text{BO}_3)_2$ shows a broad peak between 2.0 K and 3.2 K [28, 34], which aligns with our K_n and $1/T_1$ data for the liquid phase of P_1 , but not for P_2 . These discrepancies may arise from effective perturbations near the nearly degenerate EP and FP phases [3], such as proximity to the DS phase and the effects of pressure hydrostaticity, as discussed above.

With the ordering temperature suppressed below 0.3 K at 5.5 T [Fig. 3(a)], the field-induced QPT in P_1 appears to be continuous or nearly continuous. Notably, the unusually large exponent $\eta \approx 0.6$, extracted from $1/T_1 \sim T^\eta$ in P_1 , suggests the transition occurs via or near a DQCP [35, 36]. In contrast, a smaller value of $\eta \approx 0.2$ has been reported for P_2 [27], possibly due to different perturbations affecting the DQCP. Theoretically, a wide range of η values has been observed, depending on the emergent symmetries and numerical methods used [11, 12, 18, 20], which complicates direct determination of DQCP universality through theory–experiment comparisons.

Our results show that the field-induced changes in T_P and T_N are significantly stronger than the effects observed under pressure at zero field [28]. This highlights the importance of investigating experimentally and theoretically whether a multicritical point [30, 37, 38] or a quantum spin liquid [38] can be stabilized at finite fields in $\text{SrCu}_2(\text{BO}_3)_2$, as these are possible outcomes near a DQCP. Notably, the pressure-induced PS–AFM transition was achieved using a diamond anvil cell [28]. Further experiments with high hydrostatic conditions are required to revisit the zero-field case.

Summary. Our NMR study on the Shastry-Sutherland compound $\text{SrCu}_2(\text{BO}_3)_2$ under pressures up to 2.65 GPa reveals a macroscopic coexistence of two plaquette phases at low temperatures, evident from their distinct behaviors in both the ordered and plaquette liquid phases. Our measurements identify enhanced spin fluctuations in one of the plaquette liquid regimes, consistent with the plaquette liquid phase in the SSM. A field-induced EP–AFM phase transition is observed near 5.5 T, accompanied by power-law scaling behavior, $1/T_1 \sim T^{0.6}$. This finding warrants further investigation under higher pressures with improved hydrostatic conditions.

The characterization of the EP phase in $\text{SrCu}_2(\text{BO}_3)_2$, with its increasing volume fraction under pressure and signs of field-induced quantum criticality, provides a promising platform for the experimental realization of the SSM and the study of DQCP behavior through combined pressure and field tuning.

Acknowledgments. We thank Prof. Bruce Normand and Prof. Wei Li for their helpful discussions. This work was supported by the National Key Research and Development Program of China (Grant No. 2023YFA1406500) and the National Natural Science Foundation of China (Grant Nos. 12374156, 12134020, 12334008 and 12174441). A portion of this work was conducted at the Synergetic Extreme Condition User Facility (SECUF).

* wqyu-phy@ruc.edu.cn

- [1] B. S. Shastry and B. Sutherland, “Exact ground state of a quantum mechanical antiferromagnet,” *Physica B+C* **108**, 1069–1070 (1981).
- [2] A. Koga and N. Kawakami, “Quantum Phase Transitions in the Shastry-Sutherland Model for $\text{SrCu}_2(\text{BO}_3)_2$,” *Phys. Rev. Lett.* **84**, 4461–4464 (2000).
- [3] M. Moliner, I. Rousochatzakis, and F. Mila, “Emergence of one-dimensional physics from the distorted Shastry-Sutherland lattice,” *Phys. Rev. B* **83**, 140414 (2011).
- [4] M. Albrecht and F. Mila, “First-order transition between magnetic order and valence bond order in a 2D frustrated Heisenberg model,” *Europhysics Letters* **34**, 145 (1996).
- [5] S. Miyahara and K. Ueda, “Exact Dimer Ground State of the Two Dimensional Heisenberg Spin System $\text{SrCu}_2(\text{BO}_3)_2$,” *Phys. Rev. Lett.* **82**, 3701–3704 (1999).
- [6] E. Müller-Hartmann, R. R. P. Singh, C. Knetter, and G. S. Uhrig, “Exact Demonstration of Magnetization Plateaus and First-Order Dimer-Néel Phase Transitions in a Modified Shastry-Sutherland Model for $\text{SrCu}_2(\text{BO}_3)_2$,” *Phys. Rev. Lett.* **84**, 1808–1811 (2000).
- [7] A. Läuchli, S. Wessel, and M. Sigrist, “Phase diagram of the quadrumerized Shastry-Sutherland model,” *Phys. Rev. B* **66**, 014401 (2002).
- [8] P. Corboz and F. Mila, “Tensor network study of the Shastry-Sutherland model in zero magnetic field,” *Phys. Rev. B* **87**, 115144 (2013).
- [9] T. Senthil, A. Vishwanath, L. Balents, S. Sachdev, and M. P. A. Fisher, “Deconfined quantum critical points,” *Science* **303**, 1490–1494 (2004).
- [10] J. Y. Lee, Y.-Z. You, S. Sachdev, and A. Vishwanath, “Signatures of a Deconfined Phase Transition on the Shastry-Sutherland Lattice: Applications to Quantum Critical $\text{SrCu}_2(\text{BO}_3)_2$,” *Phys. Rev. X* **9**, 041037 (2019).
- [11] W.-Y. Liu, X.-T. Zhang, Z. Wang, S.-S. Gong, W.-Q. Chen, and Z.-C. Gu, “Quantum Criticality with Emergent Symmetry in the Extended Shastry-Sutherland Model,” *Phys. Rev. Lett.* **133**, 026502 (2024).
- [12] A. W. Sandvik, “Evidence for Deconfined Quantum Criticality in a Two-Dimensional Heisenberg Model with Four-Spin Interactions,” *Phys. Rev. Lett.* **98**, 227202 (2007).
- [13] A. Nahum, P. Serna, J. T. Chalker, M. Ortuño, and A. M. Somoza, “Emergent $\text{SO}(5)$ Symmetry at the Néel to Valence-Bond-Solid Transition,” *Phys. Rev. Lett.* **115**, 267203 (2015).
- [14] H. Shao, W. Guo, and A. W. Sandvik, “Quantum criticality with two length scales,” *Science* **352**, 213 (2016).
- [15] N. Ma, G.-Y. Sun, Y.-Z. You, A. Vishwanath, A. W. Sandvik, and Z.-Y. Meng, “Dynamical signature of fractionalization at the deconfined quantum critical point,” *Phys. Rev. B* **98**, 174421 (2018).
- [16] B. Zhao, P. Weinberg, and A. W. Sandvik, “Symmetry-enhanced discontinuous phase transition in a two-dimensional quantum magnet,” *Nat. Phys.* **15**, 678–682 (2019).
- [17] P. Serna and A. Nahum, “Emergence and spontaneous breaking of approximate $\text{O}(4)$ symmetry at a weakly first-order deconfined phase transition,” *Phys. Rev. B* **99**, 195110 (2019).
- [18] A. Nahum, J. T. Chalker, P. Serna, M. Ortuño, and A. M. Somoza, “Deconfined Quantum Criticality, Scaling Violations, and Classical Loop Models,” *Phys. Rev. X* **5**, 041048 (2015).
- [19] C. Wang, A. Nahum, Max A. Metlitski, Cenke Xu, and T. Senthil, “Deconfined quantum critical points: Symmetries and dualities,” *Phys. Rev. X* **7**, 031051 (2017).
- [20] Y. Q. Qin, Y.-Y. He, Y.-Z. You, Z.-Y. Lu, A. Sen, Anders W. Sandvik, C. Xu, and Z. Y. Meng, “Duality between the Deconfined Quantum-Critical Point and the Bosonic Topological Transition,” *Phys. Rev. X* **7**, 031052 (2017).
- [21] B. Zhao, J. Takahashi, and A. W. Sandvik, “Multicritical Deconfined Quantum Criticality and Lifshitz Point of a Helical Valence-Bond Phase,” *Phys. Rev. Lett.* **125**, 257204 (2020).
- [22] Z. H. Liu, M. Vojta, F. F. Assaad, and L. Janssen, “Metallic and Deconfined Quantum Criticality in Dirac Systems,” *Phys. Rev. Lett.* **128**, 087201 (2022).
- [23] Y.-R. Shu, S.-K. Jian, and S. Yin, “Nonequilibrium Dynamics of Deconfined Quantum Critical Point in Imaginary Time,” *Phys. Rev. Lett.* **128**, 020601 (2022).
- [24] H. Kageyama, K. Onizuka, Y. Ueda, T. Goto, K. Yoshimura, and K. Kosuge, “Magnetic anisotropy of $\text{SrCu}_2(\text{BO}_3)_2$ with a two-dimensional orthogonal dimer lattice,” *J. Phys. Soc. Jpn.* **67**, 4304–4305 (1998).
- [25] H. Kageyama, K. Yoshimura, R. Stern, N. V. Mushnikov, K. Onizuka, M. Kato, K. Kosuge, C. P. Slichter, T. Goto, and Y. Ueda, “Exact Dimer Ground State and Quantized Magnetization Plateaus in the Two-Dimensional Spin System $\text{SrCu}_2(\text{BO}_3)_2$,” *Phys. Rev. Lett.* **82**, 3168–3171 (1999).
- [26] M. E. Zayed, Ch. Rüegg, A. M. Läuchli, C. Panagopoulos, S. S. Saxena, M. Ellerby, D. F. McMorrow, Th. Strässle, S. Klotz, G. Hamel, R. A. Sadykov, V. Pomjakushin, M. Boehm, M. Jiménez-Ruiz, A. Schneidewind, E. Pomjakushina, M. Stingaciu, K. Conder, and H. M. Rønnow, “4-spin plaquette singlet state in the Shastry-Sutherland compound $\text{SrCu}_2(\text{BO}_3)_2$,” *Nat. Phys.* **13**, 962–966 (2017).
- [27] Y. Cui, L. Liu, H. Lin, K.-H. Wu, W. Hong, X. Liu, C. Li, Z. Hu, N. Xi, S. Li, R. Yu, A. W. Sandvik, and W. Yu, “Proximate deconfined quantum critical point in $\text{SrCu}_2(\text{BO}_3)_2$,” *Science* **380**, 1179–1184 (2023).
- [28] J. Guo, P. Wang, C. Huang, B.-B. Chen, W. Hong, S. Cai, J. Zhao, J. Han, X. Chen, Y. Zhou, S. Li, Q. Wu, Z. Y. Meng, and L. Sun, “Deconfined quantum critical point lost in pressurized $\text{SrCu}_2(\text{BO}_3)_2$,” (2023), [arXiv:2310.20128 \[cond-mat.str-el\]](https://arxiv.org/abs/2310.20128).
- [29] J. Wang, H. Li, N. Xi, Y. Gao, Q.-B. Yan, W. Li, and G. Su, “Plaquette Singlet Transition, Magnetic Barocaloric Effect, and Spin Supersolidity in the Shastry-Sutherland Model,” *Phys. Rev. Lett.* **131**, 116702 (2023).
- [30] N. Xi, H. Chen, Z. Y. Xie, and R. Yu, “Plaquette valence bond solid to antiferromagnet transition and deconfined quantum critical point of the Shastry-Sutherland model,” *Phys. Rev. B* **107**, L220408 (2023).
- [31] T. Waki, K. Arai, M. Takigawa, Y. Saiga, Y. Uwatoko,

- H. Kageyama, and Y. Ueda, “A novel ordered phase in $\text{SrCu}_2(\text{BO}_3)_2$ under high pressure,” *J. Phys. Soc. Jpn.* **76**, 073710 (2007).
- [32] K. Kodama, J. Yamazaki, M. Takigawa, H. Kageyama, K. Onizuka, and Y. Ueda, “Cu nuclear spin-spin coupling in the dimer singlet state in $\text{SrCu}_2(\text{BO}_3)_2$,” *J. Phys. Condens. Matter* **14**, L319 (2002).
- [33] C. Boos, S. P. G. Crone, I. A. Niesen, P. Corboz, K. P. Schmidt, and F. Mila, “Competition between intermediate plaquette phases in $\text{SrCu}_2(\text{BO}_3)_2$ under pressure,” *Phys. Rev. B* **100**, 140413 (2019).
- [34] J. Larrea Jiménez, S. P. G. Crone, E. Fogh, M. E. Zayed, R. Lortz, E. Pomjakushina, K. Conder, A. M. Läuchli, L. Weber, S. Wessel, A. Honecker, B. Normand, Ch. Rüegg, P. Corboz, H. M. Rønnow, and F. Mila, “A quantum magnetic analogue to the critical point of water,” *Nature* **592**, 370–375 (2021).
- [35] T. Senthil, L. Balents, S. Sachdev, A. Vishwanath, and M. P. A. Fisher, “Quantum criticality beyond the Landau-Ginzburg-Wilson paradigm,” *Phys. Rev. B* **70**, 144407 (2004).
- [36] C. Li, H. Lin, and R. Yu, “Quantum scaling of the spin lattice relaxation rate in the checkerboard J-Q model,” *J. Phys.: Condens. Matter* **36**, 355805 (2024).
- [37] D.-C. Lu, C. Xu, and Y.-Z. You, “Self-duality protected multicriticality in deconfined quantum phase transitions,” *Phys. Rev. B* **104**, 205142 (2021).
- [38] J. Yang, A. W. Sandvik, and L. Wang, “Quantum criticality and spin liquid phase in the Shastry-Sutherland model,” *Phys. Rev. B* **105**, L060409 (2022).